and successfully applied the technique to solve a structure resistant to traditional direct methods.

The probabilistic approach described in paper I aims at exploiting Patterson information, both for the renormalization of the structure factors and for modifying the phase-estimating formulae. The approach has been further developed in this paper in order to take into account experimental parameters such as position and intensity of a Patterson peak. The experimental applications described here prove that the method may be useful when the distribution of the atoms in the unit cell gives rise to a large Patterson peak originated by overlapping of several interatomic vectors.

The application of the methods to usual equal-atom structures is still questionable because supplementary information contained in one (or more) weak Patterson peak has limited influence on the triplet estimation, unless a more complete analysis of the Patterson map is made. It is in this direction that we will address our future efforts.

References

ALLEGRA, G. (1979). *Acta Cryst.* A**35**, 213-220.
BURLA, M. C., CAMALLI, M., CASCARANO, G., GIACOVAZZO, C., POLIDORI, G., SPAGNA, R. & VITERBO, D. (1989). *J. Appl. Cryst.* **22**, 389-393.
CAPASSO, S., MAZZARELLA, L., SICA, F., ZAGARI, A., CASCARANO, G. & GIACOVAZZO, C. (1991). Submitted to *Acta Cryst.* B.
CASCARANO, G., GIACOVAZZO, C. & LUIĆ, M. (1988). *Acta Cryst.* A**44**, 176-183, 183-188.
CASCARANO, G., GIACOVAZZO, C. & VITERBO, D. (1987). *Acta Cryst.* A**43**, 22-29.
COCHRAN, W. (1952). *Acta Cryst.* **5**, 65-67.
COCHRAN, W. & WOOLFSON, M. M. (1955). *Acta Cryst.* **8**, 1-12.
GIACOVAZZO, C. (1991). *Acta Cryst.* A**47**, 256-263.
HAUPTMAN, H. & KARLE, J. (1953). *The Solution of the Phase Problem. I. The Centrosymmetric Crystals.* ACA Monogr. No. 3. New York: Polycrystal Book Service.
HOPPE, W. (1963). *Acta Cryst.* **16**, 1056-1057.
KARLE, J. & KARLE, I. (1966). *Acta Cryst.* **21**, 849-859.
MAIN, P. & WOOLFSON, M. M. (1963). *Acta Cryst.* **16**, 1046-1051.
NIXON, P. E. (1978). *Acta Cryst.* A**34**, 450-453.
RIUS, J. & MIRAVITLLES, C. (1989). *Acta Cryst.* A**45**, 490-494.
STANLEY, E. (1979). *Acta Cryst.* A**35**, 966-970.
STANLEY, E. (1986). *Acta Cryst.* A**46**, 297-299.

Acta Cryst. (1992). A**48**, 36-41

Convergent-Beam RHEED Calculations of a 'Forbidden Reflection' from the Si (111) Surface

BY ANDREW E. SMITH

Department of Physics, Monash University, Clayton, Victoria 3168, *Australia*

(*Received* 24 *August* 1990; *accepted* 15 *July* 1991)

Abstract

Results of convergent-beam reflection high-energy electron diffraction (CB-RHEED) calculations are presented for the (111) surface of silicon. These double rocking calculations are performed using a dynamical scattering approach. This is based on evaluation of the surface parallel multislice matrix for reflection with account taken of the boundary conditions. In particular, calculations are shown for intensities close to a reflection that is kinematically forbidden. Particular note is made of the computational simulation of intensity enhancements corresponding to surface wave resonance conditions.

1. Introduction

Reflection electron microscopy (REM) allows the direct observation of such surface topographical details as single-atom steps, dislocations and surface particles (Yagi, 1987). The best REM contrast conditions are often achieved for incident beam angles where electron reflection is not necessarily supported by strong bulk diffraction (Uchida, Lehmpfuhl & Jager, 1984). The choice of incidence angle is then guided by surface diffraction considerations and not only by supposed satisfaction of kinematical bulk Bragg reflection diffraction.

One such incident direction which can produce a strong reflection corresponds to the so-called surface wave resonance (SWR) effect. In SWR one of the diffracted beams is trapped in a state close to the surface and is not able to propagate in vacuum. This can be understood as an Ewald-sphere tangency condition and incident conditions can be determined by a simple geometric construction (Ichimiya, Kambe & Lehmpfuhl, 1980).

Strong contrast effects in REM are also achievable by illuminating at incident conditions corresponding to 'forbidden' reflections, *e.g.* 666 for the Si (111) surface (Uchida & Lehmpfuhl, 1987). The reflection is then not directly supported by a single bulk diffraction event, but by multiple diffraction events [*Umweganregung* (von Laue, 1948)]. However, from the viewpoint of a surface diffraction process, such

0108-7673/92/010036-06$03.00 © 1992 International Union of Crystallography

a 'forbidden' reflection can be directly supported. This is because the diffraction rod corresponding to the two-dimensional surface net has always a finite scattering strength along all of its length.

Surface structure information in REM can accordingly be increased at incident directions selected on the basis of the geometry pertaining to the surface diffraction conditions. Such conditions can be more directly observed in the diffraction technique corresponding to REM, reflection high-energy electron diffraction (RHEED). RHEED is able to provide information on the crystallographic structure of surface layers and is utilized routinely as a diagnostic tool in crystal growth using molecular beam epitaxy (Neave, Joyce, Dobson & Norton, 1983).

Conventional RHEED has been extended to a 'convergent-beam' (CB) double rocking technique similar to that employed in transmission electron microdiffraction (Tanaka & Terauchi, 1985; Tanaka, Terauchi & Kaneyama, 1988). This CB-RHEED technique has been employed in both specially built diffraction cameras (Ichimiya, Kambe & Lehmpfuhl, 1980; Lehmpfuhl & Dowell, 1986) and in modern commercial microscopes (Shannon, Eades, Meichle & Turner, 1985; Peng & Cowley, 1987).

CB-RHEED experimental diffraction contrast variations have been successfully simulated by means of dynamical diffraction calculations (Smith & Lynch, 1987; Eades, Smith & Lynch, 1987; Smith, 1988; Smith & Lynch, 1988). However, these calculations were performed for incidence close to major crystallographic zone axes. It is the object of this communication to report the details of patterns obtained for considerable tilts away from a major zone-axis position. Such incident directions can correspond to simultaneous satisfaction of both SWR and forbidden reflection conditions for the Si (111) surface. A detailed comparison is then possible with the large intensity enhancements that have been observed experimentally for this surface in CB-RHEED (Lehmpfuhl & Dowell, 1986). These in turn can be directly related to the strong contrast observed in REM for the same incident angles (Uchida & Lehmpfuhl, 1987).

2. CB-RHEED geometry and principles of the calculation

RHEED spot patterns from crystal surfaces can be envisaged by the Ewald-sphere construction. Individual spots correspond to intersections of the sphere with reciprocal-lattice rods of the crystal surface. In CB-RHEED the incoming beam is no longer a single plane wave, but comprises a multiplicity of plane waves with a range of allowed incident angles defined by a limiting aperture. A CB-RHEED pattern consists of a series of patterns comprising individual RHEED spots for each of the incident directions. As long as the aperture size is small enough, the patterns for the individual rods are separated.

Owing to the reflection geometry the various rod pattern envelopes in CB-RHEED are distorted except for the specular reflected beam, which always retains the initial disc form (Shannon, Eades, Meichle, Turner & Buxton, 1984). Simple geometrical constructions can be used to determine the diffracted beam envelopes for each reciprocal-lattice rod (Shannon *et al.*, 1985; Smith & Lynch, 1987). Geometrical constructions can determine positions of surface wave resonance conditions in CB-RHEED as loci of tangency conditions for the rotating Ewald sphere (Ichimiya, Kambe & Lehmpfuhl, 1980). These can be combined with geometrical positions of the Kikuchi and Bragg conditions (Lehmpfuhl & Dowell, 1986).

Even though some positional information can be determined for features of interest by these geometrical (*i.e.* kinematical) constructions, it is necessary to perform dynamical diffraction calculations to obtain information about intensity distributions. Owing to the reflection geometry and the nature of the boundary conditions the reflection calculation is more substantial than the transmission case.

The present calculations are performed using a multislice formulation of the problem (Cowley & Moodie, 1957; Lynch & Moodie, 1972). For each slice, taken parallel to the surface, the two-dimensional Fourier components are found. After solution of the eigenvalue problem for each slice, the whole problem is solved by means of a transfer matrix method. Details have been published separately (Lynch & Smith, 1983) and are the basis of the computer codes used in the present work. They are similar to formulations by Maksym & Beeby (1981) and Ichimiya (1983, 1985). For a discussion see Kambe (1988). Other methods of RHEED calculation include a multislice method based on slicing the crystal perpendicular to the beam (Peng & Cowley, 1986) and a Bloch wave method (Ma & Marks, 1989).

Following earlier work, a slice thickness of 1/36 of a unit cell was found to be adequate. Only diffraction rods close to the Ewald sphere (modified by the crystal potential) were included. These comprised both propagating and attenuating waves (*i.e.* waves both interior and exterior to the sphere). A check on sufficiency in number of rods was made by performing recalculations with different numbers of rods (Smith, 1988; Smith & Lynch, 1988).

The scattering matrices for silicon were constructed using unit-cell parameters from Wyckoff (1963) and scattering factors for neutral silicon from Doyle & Turner (1968). Following Ino's (1977) RHEED experimental results, it was decided for simplicity to use an abrupt termination of the bulk diamond lattice, without relaxation or reconstruction, as the surface. This is an appropriate starting point for an analysis

of Lehmpfuhl & Dowell's (1986) results in view of the crystal preparation technique that was employed.

The superposition of the Si atoms using the Doyle & Turner data gave a value of 13.8 eV for the value of the zeroth-order Fourier component of the potential $V(0,0,0)$, *i.e.* the inner potential. Following experimentally measured values based on determinations of the refractive-index effect (Menadue, 1972; Ichimiya, 1987), this was changed to a value of 12 eV.

A uniform imaginary potential was adopted. This was taken to have a value of 0.7 eV as guided by transmission work (Voss, Lehmpfuhl & Smith, 1980; Ichimiya & Lehmpfuhl, 1978; Radi, 1970). Furthermore, because of cubic symmetry and in order to eliminate redundant beams, a non-conventional hexagonal unit cell was chosen (Smith & Lynch, 1988). This has hexagonal a and b axes in the surface each with cell length equal to $1/2^{1/2}$ of the conventional cell side. The perpendicular c axis has cell length equal to $3^{1/2}$ of the conventional cell length.

3. Results

For comparison with previous work (Smith & Lynch, 1988), results are first presented for incidence close to the $\langle 11\bar{2}\rangle$ zone axis. Accordingly, Fig. 1 shows results of computations on an 81×81 rectangular mesh in the display plane. It displays a three rod calculation comprising the $(\bar{1}\bar{1})$, (00) and (11) rods. In conventional notation these correspond to $2\bar{2}0$, 000 and $\bar{2}20$ reflections. Increments in display are back-transformed to the hexagonal system in order to determine the corresponding changes in tilt. The simulation is for a rectangular aperture. The azimuthal tilt is from $-\theta_B$ to θ_B, where θ_B is the Bragg angle corresponding to the $\bar{2}20$ reflection. Hence the CB-RHEED simulated patterns from the different rods just touch one another.

In terms of the nonconventional cell the colatitude tilt is from $2c^*$ to $8c^*$ with centre at $5c^*$. This corresponds in the conventional cell to a total tilt from $(\frac{2}{3}\frac{2}{3}\frac{2}{3})$ to $(\frac{8}{3}\frac{8}{3}\frac{8}{3})$. For Bragg (or Kikuchi) reflections the tilt corresponds to a lower edge of $(\frac{4}{3}\frac{4}{3}\frac{4}{3})$, an upper edge of $(\frac{16}{3}\frac{16}{3}\frac{16}{3})$ and centre at $(\frac{10}{3}\frac{10}{3}\frac{10}{3})$ (ignoring the refractive-index effect). The portions of CB-RHEED pattern for the non-specular rods corresponding to the region less than $2c^*$ are not displayed.

Fig. 2 shows results for the same incidence conditions as in Fig. 1 but with a circular aperture of radius equal to half the inter-rod distance, *i.e.* corresponding to θ_B for the $\bar{2}20$ reflection. The regions again just touch but the influence of the circular aperture on the beam envelopes of the non-specular rods now becomes apparent. The shapes are in agreement with the geometrically determined loci (Shannon *et al.*, 1985; Smith & Lynch 1987). This provides a useful check on the graphical output. Again portions of the CB-RHEED patterns less than $2c^*$ are not displayed.

Another useful check on the graphics output is provided by the direct method used in this paper to produce patterns (Smith, 1989). In some previous CB-RHEED simulations the total pattern was produced by the photomontage of individual patterns from the various rods (*e.g.* Smith & Lynch, 1988). However, in the present work simulations are achieved using a dot matrix printer to produce a

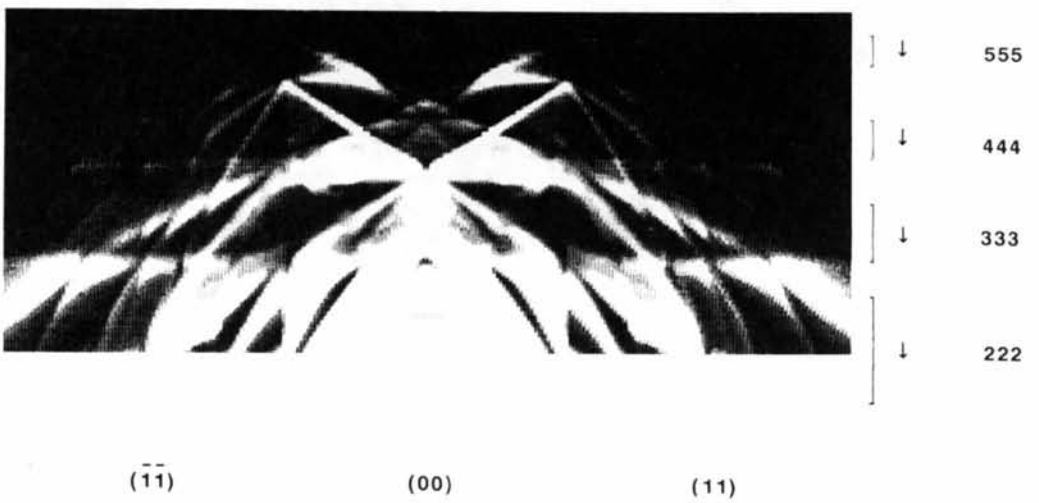

Fig. 1. Results of dynamical CB-RHEED calculations for three rods comprising: the (00) specular together with the $(\bar{1}\bar{1})$ and (11) non-speculars with incidence close to the $\langle 11\bar{2}\rangle$ zone axis for the (111) silicon surface at 80 keV incident energy. The colatitude angles of incidence cover the range $2c^*$ to $8c^*$ reciprocal-lattice vectors (non-conventional cell) with the centre of the pattern at 1.3° corresponding to $5c^*$. The central azimuthal angle is along the zone axis. The maximum azimuthal tilt is 0.8° corresponding to one half of the reciprocal-lattice rod spacing. The calculation is carried out on an 81×81 rectangular mesh with inner potential equal to 12.0 eV and absorption potential equal to 0.7 eV. Also denoted are the kinematic positions of Bragg and Kikuchi reflections from planes parallel to the surface together with their displacements due to the refractive-index effect.

logarithmic grey scale with 25 levels. Fairly large total patterns can then be formed by storing individual parts corresponding to the various directions in individual computer files. These are subsequently merged into a larger file for simultaneous display of all the results.

Fig. 3 shows the results of a calculation taken for a considerable tilt away from the $\langle 11\bar{2}\rangle$ zone axis. Again computations are for an 81×81 rectangular mesh in the display plane. However, this time the calculation contains five rods comprising the $(\bar{3}\bar{3})$, $(\bar{2}\bar{2})$, $(\bar{1}\bar{1})$, (00) and (11) rods. In conventional notation these correspond to $6\bar{6}0$, $4\bar{4}0$, $2\bar{2}0$, 000 and $\bar{2}20$ reflections. The simulation is for a rectangular aperture. The azimuthal tilt is from θ_B to $3\theta_B$ where θ_B is the Bragg angle corresponding to the $\bar{2}20$ reflection. In terms of the nonconventional cell the colatitude tilt is from $4c^*$ to $10c^*$. For Bragg (or Kikuchi) reflections this corresponds to a lower edge of $(\frac{8}{3}\frac{8}{3}\frac{8}{3})$ and an upper edge of $(\frac{20}{3}\frac{20}{3}\frac{20}{3})$ (ignoring the refractive-

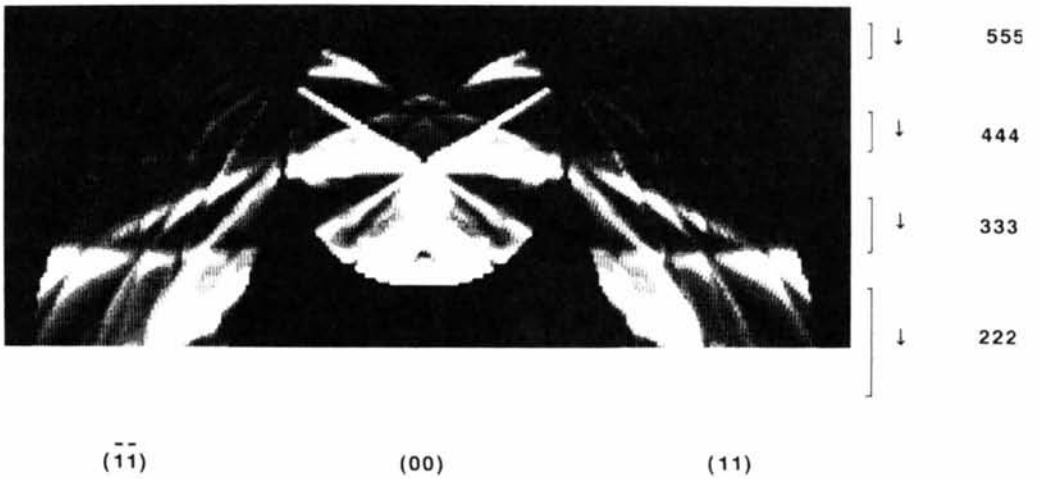

Fig. 2. Results of dynamical CB-RHEED calculations for the same parameters as in Fig. 1 but with a circular aperture in the incident beam. The colatitude angle of incidence at the centre of the circular disc defining the pattern circumference is 1.4° corresponding to $5.5c^*$ reciprocal-lattice vectors. The central azimuthal angle is set equal to zero. The aperture radius is 0.8° corresponding to one half of the reciprocal-lattice rod spacing.

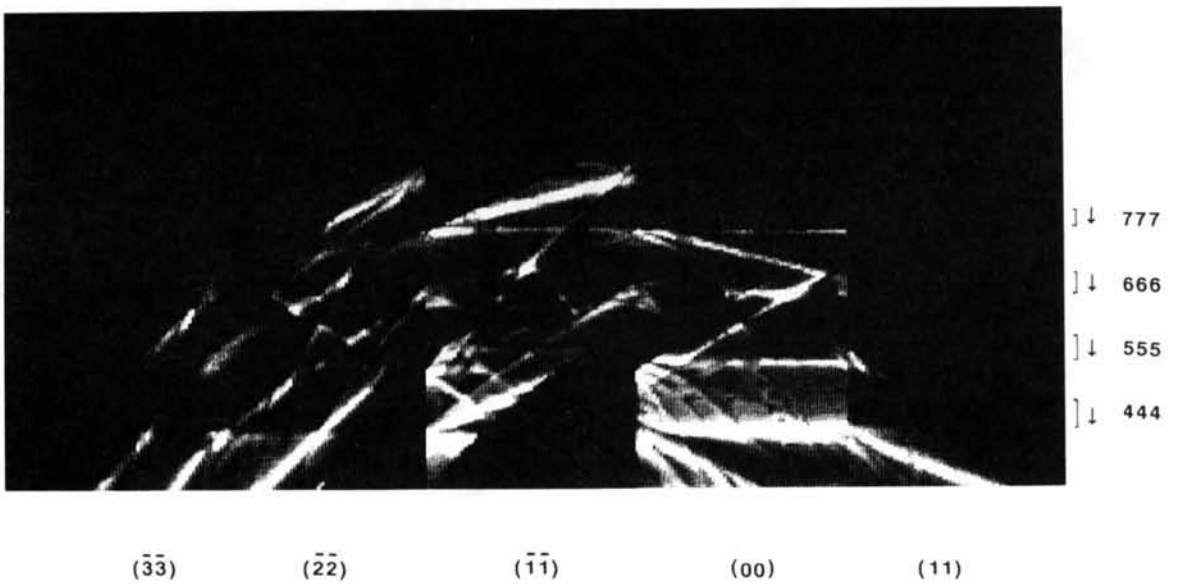

Fig. 3. Results of dynamical CB-RHEED calculations for five rods comprising: the (00) specular together with the $(\bar{3}\bar{3})$, $(\bar{2}\bar{2})$, $(\bar{1}\bar{1})$ and (11) non-speculars. The colatitude angles of incidence cover the range $4c^*$ to $10c^*$. The central azimuthal angle is directed towards the (11) rod, *i.e.* $(\bar{2}\bar{2})$ is at the Bragg position. As in the other figures, the full azimuthal tilt range corresponds to the reciprocal-lattice rod spacing. Other computational parameters as in Fig. 1.

index effect). The portions of CB-RHEED pattern for the non-specular rods corresponding to the region less than $4c^*$ are not displayed.

Fig. 4 shows results for a calculation at larger azimuthal tilts than in Fig. 3, but with similar computational parameters. In this case the azimuthal tilt is from $2\theta_B$ to $4\theta_B$ where θ_B is the Bragg angle corresponding to the $\bar{2}20$ reflection.

Figs. 1 and 2 are to be compared with the experimental pattern in Fig. 6 of Lehmpfuhl & Dowell (1986), whilst Figs. 3 and 4 are to be compared with the experimental pattern in Fig. 7 of Lehmpfuhl & Dowell (1986).

4. Comparison with geometrical patterns and refractive-index effect

In order to understand the dynamical diffraction processes observed in the CB-RHEED patterns it can sometimes be helpful to interpret features in terms of kinematic (geometric) events. However, there are displacements in position caused by the change in refractive index from vacuum to crystal. These displacements increase with diminishing incidence angles. This effect is shown in Figs. 1–4 by the displacements of kinematic Bragg (or Kikuchi) positions for diffraction from planes parallel to the surface. These features correspond to horizontal lines in the specular rod region.

These displacements are determined by means of the formula

$$\sin^2 \theta_B - \sin^2 \theta_0 = V_0/E$$

where θ_B is the Bragg angle, θ_0 is the observed vacuum angle, V_0 is the inner potential and E is the beam voltage.

In Figs. 1 and 2 refractive-index displacements downwards are shown for the 555, 444, 333 and 222 reflections. In particular, the 222 is displaced off the bottom of the diagram.

Similar refractive-index displacements are shown in Figs. 3 and 4 for the 777, 666, 555 and 444 reflections. Of particular interest are features that can be identified with the 666 reflection, as this is forbidden kinematically for the diamond structure. In the region corresponding to the specular rod a large increase in intensity can be observed close to the 666 line allowing for the refractive-index displacement. Furthermore, this occurs where a diagonal line from the bottom left to the top right cuts the horizontal line. This diagonal line has been identified as part of a parabola corresponding to a SWR (Lehmpfuhl & Dowell, 1986). The results of the present calculation agree well with experiment in respect to position and strength of this feature.

By following the increase in horizontal tilt from Fig. 3 to Fig. 4 we are able to identify the horizontal displacement of features observed in the experimental CB-RHEED pattern. The degree of agreement between calculation and experiment at the large azimuthal tilts utilized in Figs. 3 and 4 is even more striking than in the case of incidence very close to the zone axis as in Figs. 1 and 2. The large azimuthal tilt patterns no longer have the assistance of pattern symmetry to give an exaggerated impression of agreement over a sizeable incidence range.

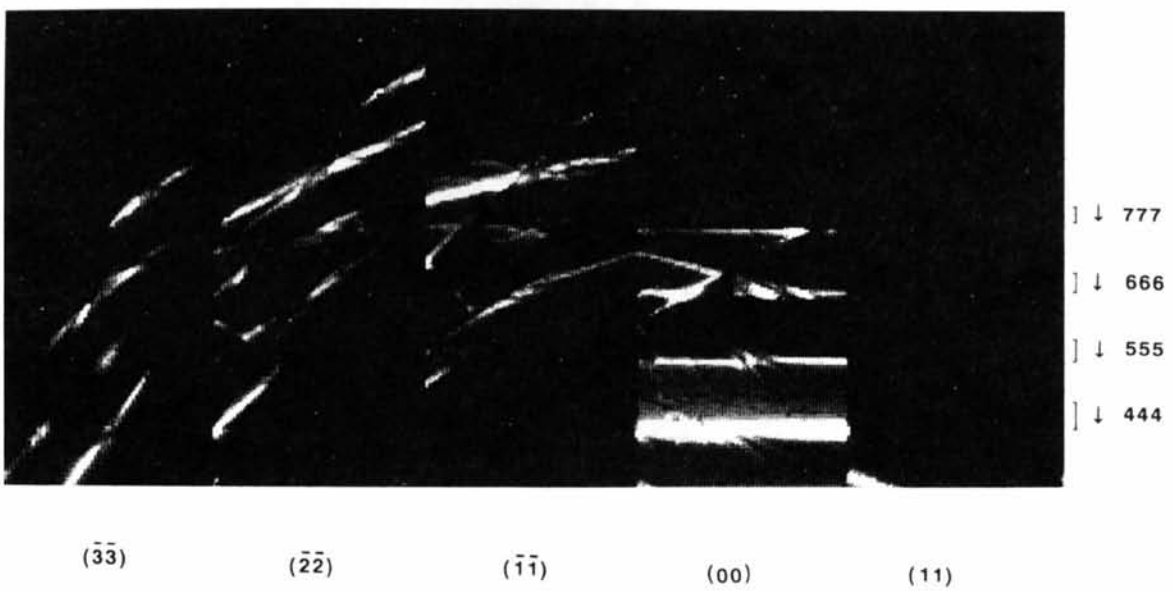

Fig. 4. Results of dynamical CB-RHEED calculations for five rods comprising: the (00) specular together with the $(\bar{3}\bar{3})$, $(\bar{2}\bar{2})$, $(\bar{1}\bar{1})$ and (11) non-speculars. The azimuthal angle closest to the $\langle 11\bar{2}\rangle$ axis is directed towards the (11) rod. As in the other figures the full azimuthal tilt range corresponds to the reciprocal-lattice rod spacing. Other computational parameters as in Fig. 1.

There is very good agreement between calculation and experiment. In particular, horizontal lines corresponding to Bragg reflections from planes parallel to the surface allow easy comparison of colatitude tilt. In addition, parabolas corresponding to both first- and second-order SWR features are reproduced in the calculations. These are the tangency conditions for the $\bar{2}20$ and $\bar{4}40$ reflections.

However, there is one feature that does not appear strongly in the experimental patterns but occurs with significant strength in the computational simulations. It is only barely discernable in the experimental results in Fig. 7 of Lehmpfuhl & Dowell (1986), although somewhat stronger in a direct print of the results. This feature is seen in Figs. 3 and 4 running diagonally from the top left to the bottom right in the specular region. It cuts the 666 line to the right of the previously mentioned intersection with the SWR parabola. This feature may be connected with a diagonal feature in the (11) rod region to the right of the specular rod region close to the bottom of Fig. 3. This calculated non-specular feature is in turn much stronger than the corresponding experimental observation, but it is very close to or below the shadow edge and accordingly would be very strongly affected by surface imperfections and protrusions. In addition, a more sophisticated surface potential than truncation, and even just incorporation of simple relaxation and reconstruction, including such features as the image potential and modification of the inelastic scattering potential might well be necessary at these extremely low angles.

Concluding remarks

Results from dynamical CB-RHEED calculations are able to simulate most of the structure and intensities seen in the corresponding experimental patterns for the silicon (111) surface. There are, however, some disagreements particularly for the outermost non-specular parts of the patterns where effects such as surface roughness and the precise form of the crystal surface potential play a particularly important part. Surface wave resonance effects are clearly identifiable in this technique. However, it is the combination of SWR with all the other dynamical scattering processes which determines the final form of the observed results. In particular, the identification of any particular 'physical' process must be viewed within all possible scattering processes.

In view of the primitive form of the inelastic potential employed in these calculations, the overall agreement between calculation and experiment is very encouraging. Work is in progress on the introduction into the CB-RHEED of a calculation scheme of inelastic potentials based on first-principle calculations (Allen & Rossouw, 1989) rather than phenomenology.

I thank Dr Denis Lynch and Dr Chris Rossouw for many fruitful discussions. In addition I thank Dr Gunter Lehmpfuhl for sending me original prints of experimental results.

The project has been supported by a Monash University Research Grant and a Monash/CSIRO Collaborative Research Grant.

References

ALLEN, L. J. & ROSSOUW, C. J. (1989). *Phys. Rev. B*, **39**, 8313-8321.
COWLEY, J. M. & MOODIE, A. F. (1957). *Acta Cryst.* **10**, 609-619.
DOYLE, P. A. & TURNER, P. S. (1968). *Acta Cryst.* A**24**, 390-397.
EADES, J. A., SMITH, A. E. & LYNCH, D. F. (1987). In *45th Annu. Proc. EMSA*, edited by G. W. BAILEY, pp. 30-33. San Francisco Press.
ICHIMIYA, A. (1983). *Jpn. J. Appl. Phys.* **22**, 176-180.
ICHIMIYA, A. (1985). *Jpn. J. Appl. Phys.* **24**, 1365.
ICHIMIYA, A. (1987). *Surf. Sci.* **192**, L893-L898.
ICHIMIYA, A., KAMBE, K. & LEHMPFUHL, G. (1980). *J. Phys. Soc. Jpn*, **49**, 684-688.
ICHIMIYA, A. & LEHMPFUHL, G. (1978). *Z Naturforsch. Teil A*, **33**, 269-281.
INO, S. (1977). *Jpn. J. Appl. Phys.* **16**, 891-908.
KAMBE, K. (1988). *Acta Cryst.* A**44**, 885-890.
LAUE, M. VON (1948). *Materiewellen und ihre Interferenzen*, 2nd ed. Leipzig: Akademische Verlagsgesellschaft.
LEHMPFUHL, G. & DOWELL, W. C. T. (1986). *Acta Cryst.* A**42**, 569-577.
LYNCH, D. F. & MOODIE, A. F. (1972). *Surf. Sci.* **32**, 422-438.
LYNCH, D. F. & SMITH, A. E. (1983). *Phys. Status Solidi B*, **119**, 355-361.
MA, Y. & MARKS, L. D. (1989). *Acta Cryst.* A**45**, 174-182.
MAKSYM, P. A. & BEEBY, J. L. (1981). *Surf. Sci.* **110**, 423-438.
MENADUE, J. F. (1972). *Acta Cryst.* A**28**, 1-11.
NEAVE, J. H., JOYCE, B. A., DOBSON, P. J. & NORTON, N. (1983). *Appl. Phys.* A**31**, 1-8.
PENG, L. M. & COWLEY, J. M. (1986). *Acta Cryst.* A**42**, 545-552.
PENG, L. M. & COWLEY, J. M. (1987). *J. Electron Microsc. Tech.* **6**, 43-53.
RADI, G. (1970). *Acta Cryst.* A**26**, 41-56.
SHANNON, M. D., EADES, J. A., MEICHLE, M. E. & TURNER, P. S. (1985). *Ultramicroscopy*, **16**, 175-192.
SHANNON, M. D., EADES, J. A., MEICHLE, M. E., TURNER, P. S. & BUXTON, B. F. (1984). *Phys. Rev. Lett.* **53**, 2125-2128.
SMITH, A. E. (1988). In *Reflection High-Energy Electron Diffraction and Imaging of Surfaces*, edited by P. K. LARSEN & P. J. DOBSON, pp. 251-258. New York: Plenum.
SMITH, A. E. (1989). *Ultramicroscopy*, **31**, 431-436.
SMITH, A. E. & LYNCH, D. F. (1987). *J. Vacuum Sci. Technol.* A**5**, 1262-1265.
SMITH, A. E. & LYNCH, D. F. (1988). *Acta Cryst.* A**44**, 780-787.
TANAKA, M. & TERAUCHI, M. (1985) *Convergent Beam Electron Diffraction*. Tokyo: JEOL.
TANAKA, M., TERAUCHI, M. & KANEYAMA, T. (1988) *Convergent Beam Electron Diffraction* II. Tokyo: JEOL.
UCHIDA, Y. & LEHMPFUHL, G. (1987). *Ultramicroscopy*, **23**, 53-60.
UCHIDA, Y., LEHMPFUHL, G. & JAGER, J. (1984). *Ultramicroscopy*, **15**, 119-129.
VOSS, R., LEHMPFUHL, G. & SMITH, P. J. (1980). *Z. Naturforsch. Teil A*, **35**, 973-984.
WYCKOFF, R. W. G. (1963). *Crystal Structures*, 2nd ed. New York: Interscience.
YAGI, K. (1987). *J. Appl. Cryst.* **20**, 147-160.